

Open-Cell Robust COF-Nanowire Network Sponges as Sustainable Adsorbent and Filter

Chenhui Ding, Yingying Du, and Seema Agarwal*

Constructing crystalline covalent organic frameworks (COF) robust 3D reusable macroscopic objects exposing more adsorption sites with high water flux for use as a filter is an unresolved challenge. A simple scalable procedure is shown for making a robust, highly compressible 3D crystalline COF nanowire interconnected porous open-cell sponge. The compressive strength and Young's modulus (80% strain) of the sponge are 175 and 238 kPa, respectively. The sponge can withstand multiple compression-release cycles and a load of 2800 times its weight without collapsing. As an exemplary application, the use of a COF sponge in the selective removal and separation of cationic model dye from a mixture of dyes in water by adsorption and filtration with >99% efficiency is shown. Depending on the dye concentration, the dye removal time can be as short as 2 min, and dye adsorption efficiency can be as high as 653 mg g⁻¹ (COF in the sponge). During filtration, the sponges as filters show a high water flux of 2355 L h⁻¹ m⁻² under ambient conditions and maintain their performance for many cycles. The lightweight, reusability, and efficiency make present sponges sustainable materials as adsorbents and filters.

1. Introduction

Covalent organic frameworks (COFs) in the last decades have become an undisputed advanced material type for wide applications in fields, such as gas storage,^[1] separation,^[2] catalysis,^[3] water purification,^[4] molecular separations,^[5] energy storage,^[6] and light-emitting diodes.^[7] Vulnerability concerning the degree of crystallinity, chemical structure, functionality, pore size, surface area, and porosity in addition to high chemical and thermal stability make COFs promising candidates for applications mentioned above. Due to their chemically cross-linked structure, they are obtained as an insoluble and infusible powder after


synthesis. The powder form makes their utility in several applications including contaminant removal from solutions non-sustainable and tedious.^[8] The separation of COF powder after use is an energy-intensive process. Further, for sustainability, it is important to reuse COFs as far as possible.^[9] In addition, the irregularly packed agglomerated COF powders reduce the accessible adsorption sites and hinder the mass transport and adsorption of contaminants, such as dyes during water purification.

Therefore, COFs in the form of self-standing robust easy-to-handle macro-objects with access to all active sites that can be easily separated and reused will be more promising.^[10] Various methods are studied to get COFs in the form of 2D membranes. For example, growing on a solid-substrate,^[11] liquid-liquid interface polymerization,^[12] phase-switching process,^[13] and template-assisted framework (TAF) process.^[14] The COF

precursors are also mixed with graphene oxide (GO)/polymer binder, freeze-dried, and heated to produce a 3D macro-object.^[15] In addition to COF precursors, readymade COF nanoparticles are also mixed with GO/polymer binders and converted to 3D objects by freeze-drying/supercritical drying.^[16] Also, melamine-formaldehyde foams coated with COF were prepared by dipping the foam into a precursor solution of COF followed by heating.^[17] Pure COF 3D macro-objects in general are mechanically brittle and show shrinkage during preparation. Tian et al. grew COF in situ on the microporous channels of wood to obtain wood/COF composites.^[18] The robust wood skeleton ensures the recyclability of the composite material. However, due to the lack of strong force between COF and wood, the COF powder does not completely cover the surface of the wood, and the wood itself does not have a highly interconnected porous structure, which limits the diffusion of organic pollutants.

COFs are advanced materials showing benefits as porous adsorbents, a property that is highly useful for the removal of pollutants.^[19] In the form of self-standing robust 3D macro-objects COFs can provide additional advantages of ease of separation, reusability, and excellent mass transfer in applications like pollutant removal. Therefore, the design of COF macro-objects as adsorbents should include some important aspects: robustness (mechanical stability), high porosity, and open inter-connected porous structure to ensure the rapid mass transfer and recycling

C. Ding, Y. Du, S. Agarwal
Macromolecular Chemistry and Bavarian Polymer Institute
University of Bayreuth
Universitätsstrasse 30, 95440 Bayreuth, Germany
E-mail: agarwal@uni-bayreuth.de

 The ORCID identification number(s) for the author(s) of this article can be found under <https://doi.org/10.1002/adfm.202309938>

© 2023 The Authors. Advanced Functional Materials published by Wiley-VCH GmbH. This is an open access article under the terms of the Creative Commons Attribution License, which permits use, distribution and reproduction in any medium, provided the original work is properly cited.

DOI: 10.1002/adfm.202309938

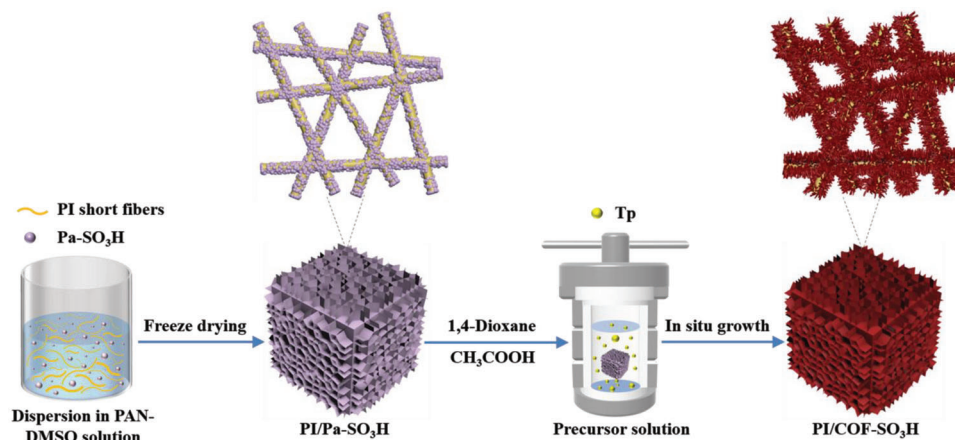


Figure 1. Schematic illustration of the preparation of polyimide / sulfonic acid functionalized COF composite sponges (PI/COF-SO₃H). PI = polyimide, PAN = polyacrylonitrile, Pa-SO₃H = 2,5-diaminobenzenesulfonic acid, Tp = 1,3,5-triformylphloroglucinol, DMSO = dimethylsulfoxide, CH₃COOH = acetic acid.

of adsorbent, the availability of COF adsorbing sites not only on the surface but also in the bulk of 3D macro-objects, and appropriate functionality to improve the adsorption capacity. Besides this, the production of 3D COF macro-objects should be up scalable, and easy. The prime challenge is to prepare such a robust crystalline COF macro-object fulfilling all these requirements. For wastewater purification applications, in addition, a large water flux through 3D macro-objects should also be secured by a tailor-made COF structure.

3D electrospun short fiber sponges with high porosity, good mechanical properties, and highly interconnecting porous structure have been applied in oil-water separation, protein purification, and seawater desalination, and show high stability and high flux.^[20] Previously we established preparation methods for such sponges from short electrospun fibers in our group.^[21] The compressible, robust sponges are formed by the percolation of short electrospun fibers during freeze-drying giving a dual porous structure: small pores between the fibers in the sponge cell walls and big pores ($\approx 100 \mu\text{m}$) formed by sublimation of ice during freeze-drying. Such sponges should be an ideal candidate as the skeleton for the preparation of robust 3D COF crystalline macro-objects. The continuous growth of COF not only on the surface but also in the bulk is expected from the electrospun skeleton sponge structure and pore size.

In this work, we show first the preparation of robust polyimide (PI)/sulfonic acid functionalized crystalline COF nanowire (PI/COF-SO₃H) composite sponges with highly interconnected open-cell structures. Since composite sponge structure and functionality are highly promising for high water flux, mass transfer, and adsorption of selective organic dyes from water, methylene blue removal from the water was studied as an exemplary example. Also, the selectivity of the sponges for the adsorption of positively charged dye from a mixture of dyes is investigated. The superiority of present COF sponges is evident from high adsorption, high selectivity and filtration efficiency, high water flux, and reusability. The sponge preparation procedure is simple, scalable and opens up new avenues for materials not only for water purification but several other applications.

2. Results and Discussion

The open-cell porous sponges were prepared through two steps of template sponge construction using PI short electrospun fibers and in situ growth of COF, as shown in **Figure 1**.

First, PI short fibers (average diameter $d = 526 \pm 98 \text{ nm}$, average fiber length $L = 77 \pm 23 \mu\text{m}$, Figure S1, Supporting Information), and Pa-SO₃H were dispersed in a solution of PAN in DMSO by stirring at high speed, and a porous spongy template (PI/Pa-SO₃H) was constructed by freeze-drying. During freeze-drying self-assembly of PI short fibers and their percolation provides an open-cell sponge with interconnected pores (**Figure 2a-d**). PAN, as a binder, further ensured the stability of the sponge and provided a site for the growth of COF. Instead of PI, any other polymer can also be used if stable under solution and temperature conditions used for growing COF.

In the second step, COF was grown in situ on the template sponge in the form of nanowires by solvothermal method by letting Pa-SO₃H on the template sponge react with Tp. The resulting sponge is designated as PI/COF-SO₃H sponge (**Figure 2e-h**). The optical pictures of the template PI/Pa-SO₃H and PI/COF-SO₃H sponges are shown in **Figure 2a-e**. There was a color change to red due to the formation of COF on the PI/Pa-SO₃H template sponge.

PI/COF-SO₃H sponges were prepared using different loading of Pa-SO₃H in template PI/Pa-SO₃H sponges. Depending upon the amount of Pa-SO₃H loading the sponges are designated as PI/Pa-SO₃H-X and PI/COF-SO₃H-X, respectively. X (0.5, 1.0, 1.5, and 2.0) is the mass ratio of Pa-SO₃H and PI short fibers. The SEM images of PI/Pa-SO₃H sponges with different loadings of Pa-SO₃H are shown in (**Figure S2**, Supporting Information) and the corresponding COF decorated sponges (PI/COF-SO₃H) are shown in **Figure S3** (Supporting Information). The growth of COF in the form of nanowires (average diameter $d = 59 \pm 17 \text{ nm}$) was obvious from the SEM images. The growth of COF in the form of nanowires is generally rare. This morphology is achieved in literature by special modifications and methods, such as core-planarity and interfacial synthesis methods.^[22] The nanowire COF morphology is the result of

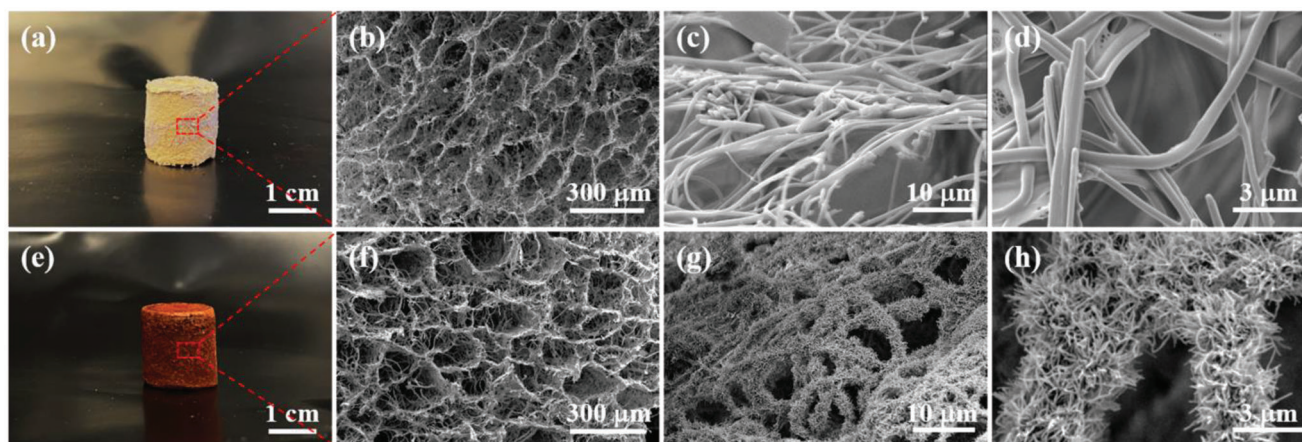


Figure 2. a–d) Photographs and SEM images of PI/Pa–SO₃H-2.0, and e–h) PI/COF–SO₃H-2.0.

the preferred growth along the *z*-direction in comparison to the *x* and *y* directions due to the stronger π – π interactions among the layers. In the work of Luo et al. COFwase assembled in the form of 1D structure, supposedly due to the special arrangement of –SO₃H in the different layers in an opposite mode rather than the common same-side mode.^[23] In our case, it might be a combination of π – π interactions and a special arrangement of –SO₃H.

The increased amount of Pa–SO₃H on the surface of PI short fibers led to the growth of denser COF and more nanowires, and the density of the PI/COF–SO₃H sponge also increased (Tables S1 and S2, Supporting Information). Although, the density of PI/COF–SO₃H-0.5 was 11.2 mg cm^{–3}, whereas it increased to 34.8 mg cm^{–3} for PI/COF–SO₃H-2.0 still the sponges are lightweight.

The cross-sectional investigations by SEM showed the growth of COF not only on the surface of the template PI/Pa–SO₃H but throughout the bulk.

Figure 3a and **Figure S4a** (Supporting Information) show the Fourier-transform infrared (FT-IR) spectra of the samples. First, characteristic peaks of PI (C=O at 1719 cm^{–1}, C–N at 1370 cm^{–1}), and PAN (C≡N at 2242 cm^{–1}) were found in all composite sponges.^[24] Second, PI/Pa–SO₃H showed obvious characteristic peaks of Pa–SO₃H (–NH₂ at 3300–35 000 cm^{–1}, –SO₃H at 1082 and 1024 cm^{–1}).^[25] Finally, with the growth of COF–SO₃H in situ, the characteristic peaks at 3300–3500 cm^{–1} (–NH₂) disappeared, and the new characteristic peaks were displayed at 1574 cm^{–1} (C=C) and 1236 cm^{–1} (C–N), indicating that conversion of PI/Pa–SO₃H to PI/COF–SO₃H.^[26] The formation of COF–SO₃H was further characterized by ¹³C cross-polarized magic angle spinning (CP MAS) NMR spectra. The chemical structures with carbon numbered and the corresponding NMR are given in **Figure 3b,c**. The characteristic peaks of PI and Pa–SO₃H were seen in the PI/Pa–SO₃H sponge. As the reaction progresses for the formation of PI/COF–SO₃H, the characteristic peaks of Pa–SO₃H disappear and typical COF–SO₃H resonances such as imine carbon peaks (≈147 ppm) and carbonyl carbon peaks (≈184 ppm) were observed in PI/COF–SO₃H sponge.^[27]

The powder X-ray diffraction (PXRD) patterns of COF–SO₃H powder and PI/COF–SO₃H sponges are shown in **Figure 3d** and **Figure S4b** (Supporting Information). It can be found that

the peaks of COF–SO₃H at $2\theta = 4.8^\circ$ (100), 8.2° (210), and 27.1° (001) are in good agreement with the simulated AA stacking model, and consistent with the literature reports for COF powder.^[28] The reflection at $2\theta = 17.2^\circ$ was attributed to PAN, whereas no peak of PI was found because it was a non-crystalline polymer.

PI/COF–SO₃H sponges are super hydrophilic as tested by contact angle measurements (water contact angle of 0°). The water penetrates the sponge instantly, as shown in Video S1 (Supporting Information). At the same time, **Figure S5** (Supporting Information) shows the thermogravimetric analysis curves of PI/COF–SO₃H sponges under a nitrogen atmosphere. PI/COF–SO₃H sponges show good thermal stability, with almost no mass loss before 200 °C, which provides the possibility for their application in high-temperature environments.

Excellent mechanical properties and good deformation recovery performance provide a guarantee for the reusability of PI/COF–SO₃H sponges. **Figure 4** shows the recovery performance (50% strain) and compressive strength (80% strain) of different composite sponges, which are summarized in Table S3 (Supporting Information). It can be found that all composite sponges exhibit good mechanical properties and deformation recovery performance, and there is no obvious change in the maximum stress and recovery height after 50 compression-release cycles (50% strain). The addition of COF greatly improved the compressive strength and deformation recovery performance of the PI/COF–SO₃H sponge. Compared with PI/COF–SO₃H, the compressive strength and Young's modulus (80% strain) of PI/COF–SO₃H-2.0 increased from 47 to 175 kPa and 46 to 238 kPa, respectively. This indicates that the highly interconnected porous structure of PI/COF–SO₃H can effectively absorb and release stress, and thus withstand multiple compression-release cycles. The dense COF nanowires grown on the surface of PI fibers serve as a protective layer, which further strengthens the fiber network framework, thereby improving the compressive strength and deformation recovery performance of PI/COF–SO₃H sponges. In addition, 71.4 mg of PI/COF–SO₃H-2.0 can withstand a weight (200 g) of 2800 times its weight without collapsing, further demonstrating its excellent compression resistance (**Figure 4g**).

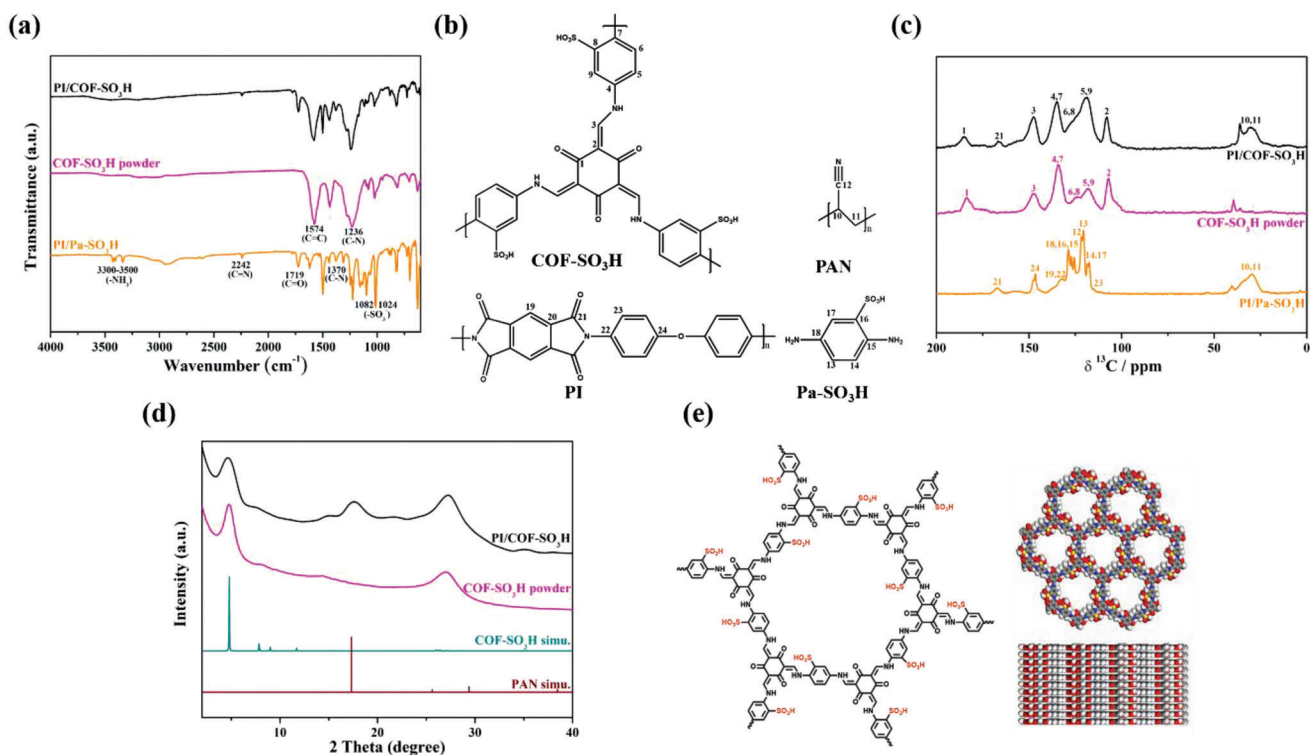


Figure 3. a) Chemical structural formulas of COF-SO₃H, PAN, Pa-SO₃H, and PI. b) FT-IR spectrum of PI/Pa-SO₃H sponge, COF-SO₃H powder, and PI/COF-SO₃H sponge. c) ¹³C CP MAS NMR spectra of PI/Pa-SO₃H sponge, COF-SO₃H powder and PI/COF-SO₃H sponge. d) PXRD patterns of COF-SO₃H powder, PI/COF-SO₃H sponge, and simulated PXRD patterns of PAN and COF-SO₃H. e) The structure and space-filled model of COF-SO₃H.

As COF-SO₃H contains a sulfonic acid group, the average Zeta potential measured on COF powder is -76.9 mV (Figures S6 and S7, Supporting Information), showing negative charge characteristics, which makes it appropriate for the adsorption of cationic dyes such as methylene blue (MB).^[29] Therefore, MB was used as the toxic model substance in this work. First, the adsorption capacity of different PI/COF-SO₃H sponges for MB was explored by taking a definite amount of the sponge (10 mg) and using 100 mL (20 mg L⁻¹) MB solution as shown in **Figure 5**. The remaining concentration of MB in the solution after 4 h was calculated using a calibration curve based on absorbance at 664 nm versus concentration by a UV-vis spectrophotometer (Figure S8, Supporting Information). The MB adsorption capacity (calculated using the total mass of the sponge) increased with the increased content of COF in the sponge. The maximum dye adsorption capacity and removal efficiency were 197.2 mg g⁻¹ (sponge) and ≈99% for PI/COF-SO₃H/COF-SO₃H-2.0, respectively. The blank sponge prepared with PI-PAN without any COF was also tested for MB adsorption and showed negligible adsorption (Figure S9, Supporting Information). Since the COF is the actual active species in the sponge responsible for the dye removal, the corresponding dye adsorption capacity was also calculated using the actual amount of the COF in the sponges. The COF in sponges showed an extremely high adsorption capacity of ≈350 mg g⁻¹ (COF in sponge) under the mentioned experimental conditions (Figure S10, Supporting Information).

Further, taking PI/COF-SO₃H-2.0 as a representative candidate, the concentration of residual dye in the solution at different time intervals was determined, and the adsorption kinetics of MB were obtained, as shown in **Figure 6a**. It can be seen that the adsorption capacity of PI/COF-SO₃H-2.0 for MB increases significantly within the first 60 min, and increases with the contact time within 180 min, after which the adsorption equilibrium is reached. To explore the possible adsorption mechanism of MB by PI/COF-SO₃H-2.0 different probable kinetic models as suggested in the literature were fitted (Figure 6b-d; Table S4, Supporting Information).^[30] The pseudo-second-order kinetic model with a higher correlation coefficient ($R^2 = 0.9865$), and a more consistent dye adsorption capacity (q_e) theoretical value with the experimental value is the best fit. The pseudo-second-order kinetic model is based on the assumption that the adsorption rate is controlled by chemisorption.^[31] Therefore, the adsorption behavior of MB on PI/COF-SO₃H-2.0 is most probably chemisorption.^[32] Further, the plot of dye adsorption capacity at any particular time (t) versus $t^{1/2}$ showed two distinct stages. In the first stage, a fast adsorption rate and a large slope of the curve are seen. The highly interconnected open-cell structure of PI/COF-SO₃H-2.0 and a large number of negatively charged functional groups on the surface most probably accelerated the diffusion and adsorption of MB on the COF surface. In the second stage, MB molecules pass from the surface of the COF to the interior through the nanochannel, and there is a repulsive force between MB molecules, which increases the diffusion resistance

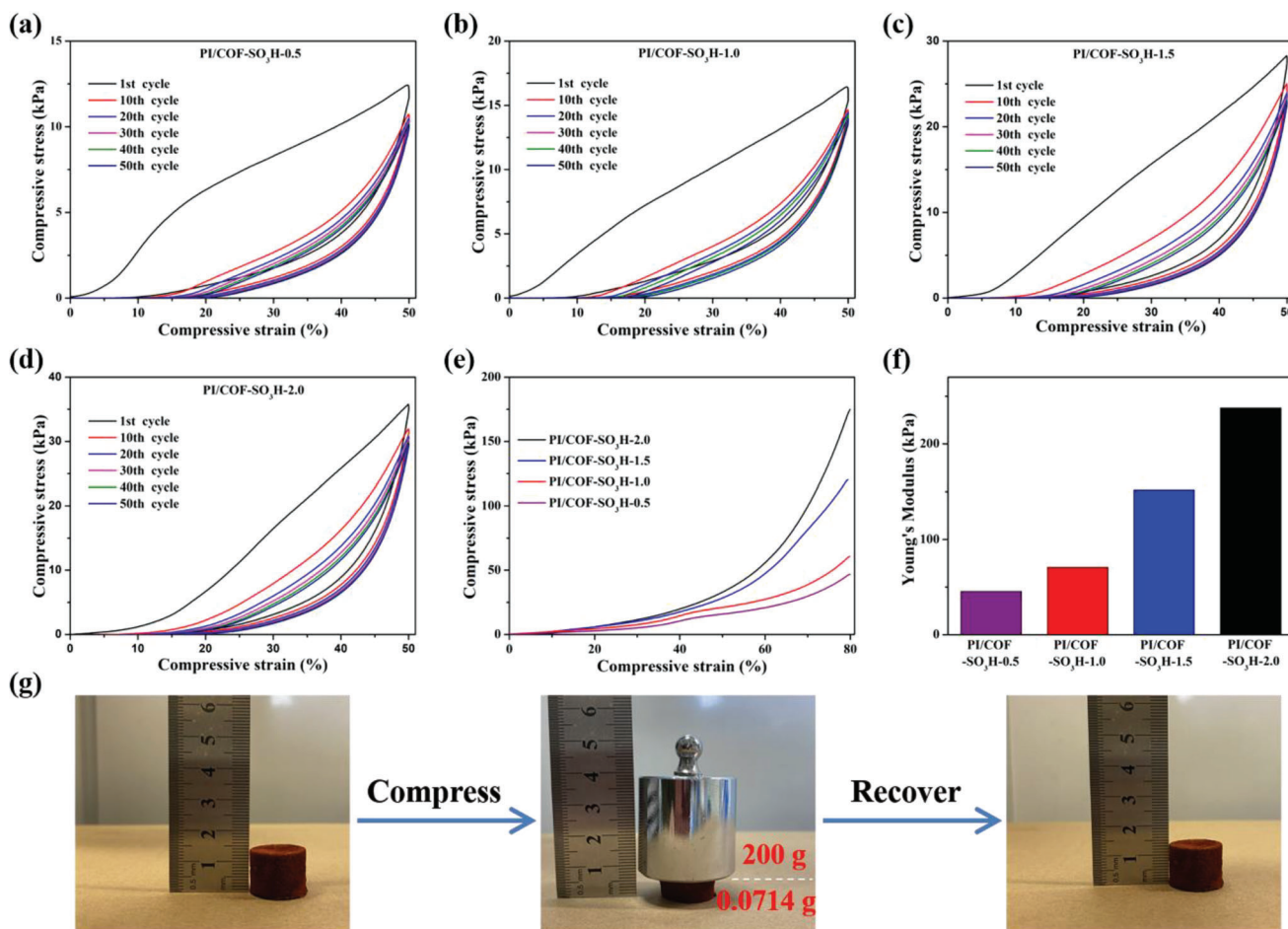


Figure 4. a–e) Compression–release stress–strain and compressive stress–strain curves of PI/COF–SO₃H sponges, f) the corresponding compressive Young's modulus, g) and compressive capacity (weight load test) of PI/COF–SO₃H-2.0.

and reduces the diffusion rate, resulting in a decreased slope of the curve.

To compare the dye removal efficiency of COF powder and COF immobilized on sponges, an experiment was done using 10 mg PI/COF–SO₃H-2.0 sponge and 5.84 mg of the COF powder for the removal of MB from 5 mL water solution of MB concentration 20 mg L⁻¹ (Figure S11, Supporting Information). 5.84 mg of the COF powder was used for the experiment as

10 mg of PI/COF–SO₃H-2.0 sponge has 5.84 mg of the active MB adsorbing COF. Rapid separation of MB was observed by the sponge (≈99.5% removal of MB in 2 min), whereas, at the same time, the removal efficiency of COF powder was ≈80%. This may be because the highly interconnected open-cell structure of PI/COF–SO₃H sponges is conducive to the rapid diffusion of dyes, and COF nanowires uniformly grow on the surface of PI short fibers, exposing more adsorption sites.

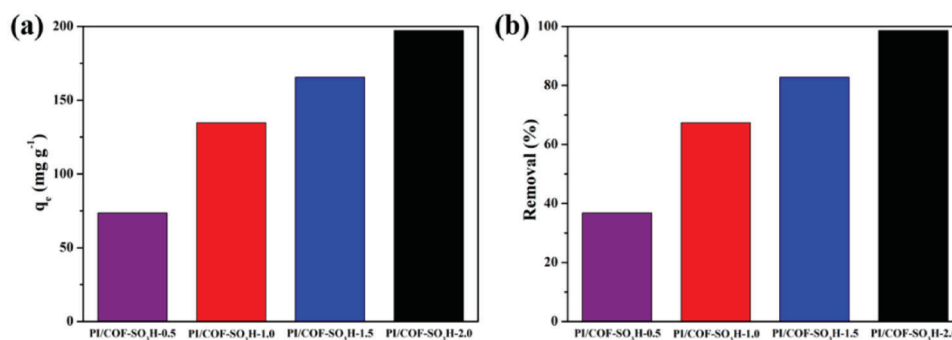


Figure 5. a) Adsorption capacity, and b) removal efficiency of MB by PI/COF–SO₃H sponges.

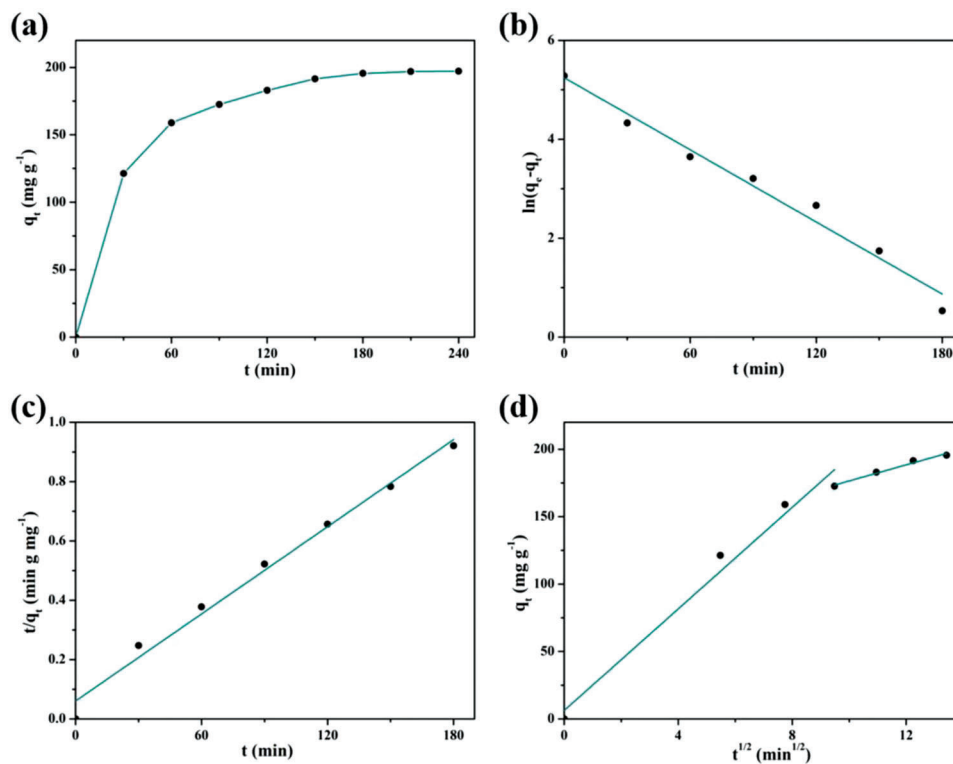


Figure 6. a) The adsorption capacity of PI/COF–SO₃H-2.0 for MB as a function of time. b) The data fitted to the pseudo-first-order kinetic model, c) the pseudo-second-order kinetic model, and d) the intra-particle diffusion kinetic model.

In additional experiments, the PI/COF–SO₃H-2.0 (10 mg) was immersed in MB solution with different initial dye concentrations (20–400 mg L⁻¹), and the concentration of residual dye in the solution after reaching adsorption equilibrium was determined. As shown in **Figure 7**, with the increase of dye concentration in MB solution, the dye adsorption capacity of PI/COF–SO₃H-2.0 first increased and then approached equilibrium, with the maximum dye adsorption capacity of ≈379 mg g⁻¹ (sponge). Taking into account that the actual amount of COF in

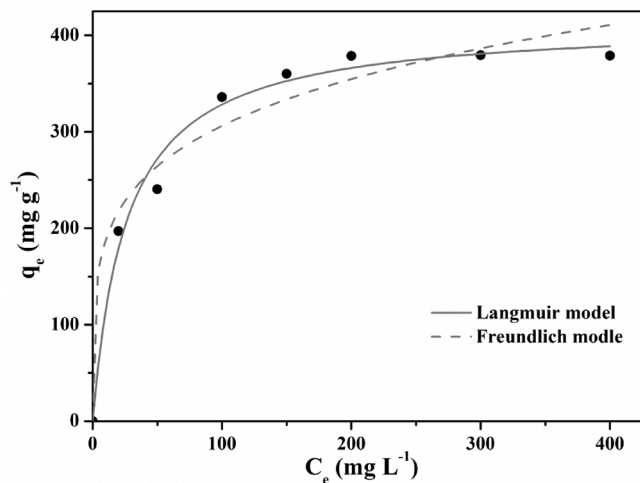


Figure 7. Equilibrium adsorption isotherm of MB on PI/COF–SO₃H-2.0.

the sponge is only 0.58 g, the actual dye adsorption capacity is ≈653 mg g⁻¹ (COF-in sponge). Meanwhile, Langmuir and Freundlich isotherm models were introduced to fit the adsorption data,^[33] and the adsorption isotherm was constructed (the fitting data is summarized in Table S5, Supporting Information). It can be found that the correlation coefficient ($R^2 = 0.9845$) of the Langmuir model is larger than that of the Freundlich model, and the theoretical value of maximum adsorption capacity is 413.93 mg g⁻¹ (sponge), which is closer to the experimental value and can accurately explain the experimental data. The Langmuir isothermal model is suitable for monolayer adsorption, which indicates that the adsorption of MB by PI/COF–SO₃H-2.0 is monolayer adsorption.^[34]

The pH value affects the surface charge of the adsorbent and dye molecules and is a key factor in adsorption experiments. The effect of pH value on the dye adsorption performance of PI/COF–SO₃H-2.0 was further explored. Wherein, 10 mg of PI/COF–SO₃H-2.0, 200 mL (20 mg L⁻¹) MB solution was taken, and the pH value of the solution was adjusted to 3–11 by adding 0.1 M HCl or 0.1 M NaOH. From Figure S12 (Supporting Information), it can be found that increasing the pH value can effectively increase the adsorption capacity of PI/COF–SO₃H-2.0 for MB, and the maximum dye adsorption capacity is 231.3 mg g⁻¹ was observed under alkaline conditions. The same sponge showed a dye adsorption capacity of <100 mg g⁻¹ under acidic conditions. This is because the surface of COF contains a large number of anionic groups, and the electrostatic interaction plays an important role in the adsorption of cationic dye MB. When the MB solution is acidic, a large number of hydrogen ions in

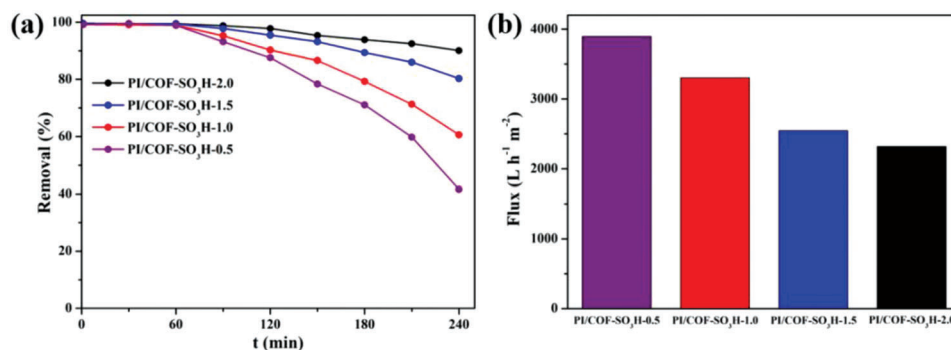


Figure 8. a) Filtration removal efficiency, and b) water flux of MB by PI/COF–SO₃H sponges.

the solution compete with MB and protonate the sulfonic acid group, repelling MB, and resulting in a low adsorption capacity of PI/COF–SO₃H-2.0 for MB. When the MB solution is alkaline, a large amount of hydroxide ions in the solution is conducive to the ionization of the sulfonic acid groups on the surface of COF, which makes it easier to adsorb MB.^[35] Therefore, a neutral or alkaline MB solution is more conducive to the adsorption of MB by PI/COF–SO₃H-2.0.

Due to the mechanical robustness of the sponges, they can also be used as filters. Therefore, a simple filtration device is constructed by placing cylindrical PI/COF–SO₃H sponges in a syringe, as shown in Figure S13a (Supporting Information). Due to the highly interconnected open-cell structure of the PI/COF–SO₃H sponges, no external driving force is required, and the dye solution could pass through the PI/COF–SO₃H sponges by its gravity and get to the clarified water, as shown in Video S2 (Supporting Information). The loading capacity of COF affects the structure and the dye adsorption capacity of PI/COF–SO₃H sponges and further affects the filtration performance of PI/COF–SO₃H sponges for MB solution. Therefore, the filtration performance of MB solution with different PI/COF–SO₃H sponges was investigated. As can be seen from **Figure 8**, the removal efficiency of MB for all composite sponges is over 99%. At the same time, all the composite sponges showed high water flux. The worth noting is the high water flux without the development of any back pressure. Once the COF in sponge filters is saturated with MB, the filtration efficiency decreased. PI/COF–SO₃H showed after 4 h of filtration still a very high dye removal efficiency of ≈90%. The proof-of-concept shows the possibility of technological upgrading in the future.

Also, in a laboratory experiment, to satisfy the long-term continuous filtration of MB solution by PI/COF–SO₃H sponges, four filtration devices (each having ≈60 mg of the sponge) are connected in series, as shown in Figure S13b (Supporting Information). For sustainable optimum use, sponge filters can also be used in modular form attaching them in a sequence at different times of filtration. Using PI/COF–SO₃H-2.0 as a filter, the whole filter device worked continuously for 24 h. The system showed excellent filtration performance (removal efficiency was 99.3%) for MB solution up to 12 h (Figure S14, Supporting Information) with a water flux of 2355 L h⁻¹ m⁻² that is far superior to COF nanofiltration membranes.^[36] Therefore, the filter device based on PI/COF–SO₃H sponges can process large quantities of MB solution quickly and efficiently.

Due to its excellent mechanical properties and good deformation recovery, PI/COF–SO₃H sponges could be regenerated after use. The reusability of regenerated PI/COF–SO₃H-2.0 as adsorbent and filter was also explored (Figure S15, Supporting Information). The PI/COF–SO₃H-2.0 has been regenerated by stirring in a methanol solution having 1 mM HCl. The regenerated sponge maintained extremely high MB removal efficiency even after 10 cycles for both as adsorbent and filter. Moreover, the MB adsorption and recycling performance of PI/COF–SO₃H sponge were compared with other works of literature (Table S6, Supporting Information). The results show that the PI/COF–SO₃H sponge exhibits a combination of high adsorption capacity and excellent recycling performance.

Due to the –SO₃H groups in COF, the present sponges can also be used for the separation of oppositely charged dyes by specifically adsorbing only positively charged dye. Therefore, in an experiment with the negative fluorescein sodium salt (FL), the PI/COF–SO₃H-2.0 sponge retained only 8% of the dye as measured by the absorbance at 490 nm by UV–vis spectroscopy (Figure S16, Supporting Information). Further, the anionic dye FL was mixed with MB to explore the selectivity of our sponge filter (**Figure 9a**; Video S3, Supporting Information). The mixed dye solution was green in color, whereas pure FL solution had yellow color and MB had blue color. The first indication of the dye separation was the change in the color from green to yellow of the solution eluting out from the filter. The yellow color is consistent with the initial FL solution color, and the absorbance of FL at 490 nm remains unchanged (Figure 9b). No absorbance of MB at 664 nm was seen in the eluted solution showing efficient separation of dyes.

3. Conclusion

A simple method of making robust, compressible 3D COF macro-object with an open-cell structure (sponge) is established in the present work. The COF nanowires were grown on a template light-weight sponge prepared from short electrospun fibers. Since the process of electrospinning and freeze-drying (the methods used in the preparation of the sponge) on a large scale are possible, the present method of making PI/COF–SO₃H will be up scalable. The chemical functionality and the network framework structure in sponges are ideally suitable for use as adsorbents and filters. The maximum adsorption capacity of PI/COF–SO₃H-2.0 to MB reached ≈653 mg g⁻¹ (COF-in sponge). Compared

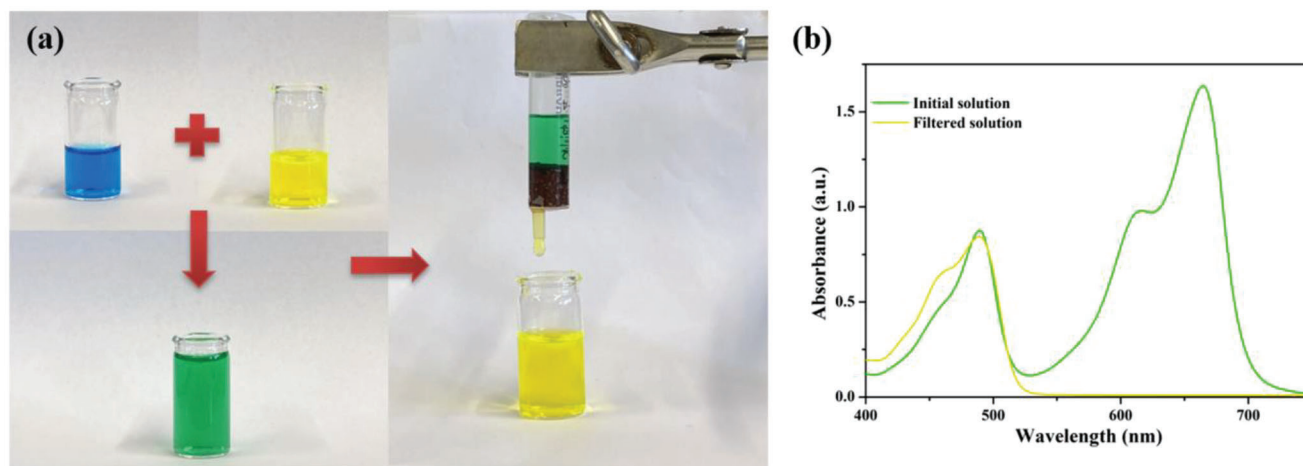


Figure 9. a) Selective filtration separation of a mixed solution of MB and FL by PI/COF-SO₃H-2.0. b) UV-vis spectra of the mixed dye solution before and after filtration.

with COF-SO₃H powder, PI/COF-SO₃H-2.0 was able to remove MB faster (99.5% removal within 2 min). In addition, using PI/COF-SO₃H sponges as a filter, high dye removal efficiency (99.3%), high flux (2355 L h⁻¹ m⁻²), and rapid adsorption and separation of a mixture of dyes were possible. Meanwhile, in the adsorption and filtration experiments, PI/COF-SO₃H sponges still exhibited excellent dye removal performance after 10 cycles of regeneration.

4. Experimental Section

Materials and Chemicals: Electrospun polyimide (PI) short fiber from Jiangxi Xiancai nanofiber Technology Co.Ltd. Polyacrylonitrile (PAN, Mw = 80 000, Carl Roth), 2,5-Diaminobenzenesulfonic acid (Pa-SO₃H), 1,3,5-triformylphloroglucinol (Tp), methylene blue (MB, powder), and fluorescein sodium salt (FL, powder) were purchased from Sigma-Aldrich. Dimethyl sulfoxide (DMSO, 99.9%), 1,4-Dioxane (99.9%), and acetic acid (AcOH, 99.7%) were purchased from Fisher Chemical. All chemicals were used directly without further purification.

Preparation of the PI/COF-SO₃H Sponges: The PI/COF-SO₃H sponges were prepared in two steps, as shown in Figure 1. The first step was to construct the PI/Pa-SO₃H sponges: 100 mg of PI short fibers, 100 mg of PAN powder, and a certain amount of Pa-SO₃H (50, 100, 150, and 200 mg) were uniformly dispersed in 25 g of DMSO by high-speed stirring, and the PI/Pa-SO₃H sponges were obtained after freeze-drying. Depending upon the amount (X is the mass ratio of Pa-SO₃H and PI short fibers, X = 0.5, 1.0, 1.5, and 2.0) of Pa-SO₃H loading the sponge was designated as PI/Pa-SO₃H-X. The second step, in situ growth of COF-SO₃H: take PI/Pa-SO₃H-2.0 as an example. The PI/Pa-SO₃H-2.0 (400 mg) was added to a 1,4-Dioxane (74.4 g) solution containing Tp (148.8 mg) and acetic acid (1.48 g) and reacted at 120 °C for 3 days to obtain dark red PI/COF-SO₃H-2.0. Then it was washed multiple times with 1,4-Dioxane and acetone, and dried under vacuum at 60 °C for 24 h. The prepared composite sponges were named PI/COF-SO₃H-0.5, PI/COF-SO₃H-1.0, PI/COF-SO₃H-1.5, and PI/COF-SO₃H-2.0, respectively. And, by measuring the weight change of the composite sponge before and after growing COF, the weight ratio of each component can be obtained, which is summarized in Tables S1 and S2 (Supporting Information). Also, prepare a PI-PAN blank sponge without any COF using the same method.

Synthesis of COF-SO₃H Powder: Tp (63 mg (0.3 mmol)) and 84.7 mg (0.45 mmol) of Pa-SO₃H were added into an autoclave with 1,4-dioxane (31.5 mg) and acetic acid (0.63 mg) reacted at 120 °C for 3 days. The result-

ing dark red product was washed multiple times with DMSO, 1,4-dioxane, and acetone, and dried under vacuum at 60 °C for 24 h.

Batch Adsorption and Continuous Filtration Experiments: The absorbance at the maximum absorption wavelength (664 nm for MB) of MB solutions with standard concentrations of 0.1, 0.2, 0.5, 1, 2, and 3 mg L⁻¹ was measured by a UV-vis spectrophotometer, and the standard curve and fitting equation was obtained.

The adsorption capacity of different composite sponges on MB was explored. At room temperature, soak 10 mg of adsorbent in 100 mL of MB solution (20 mg L⁻¹, pH value was 7), place it on a stirrer with a rotation speed of 200 rpm, until the adsorption equilibrium is reached, and use UV-vis spectroscopy to determine the residual dye in the solution. The concentration of the solution was obtained according to the standard curve and the fitting equation. The dye adsorption capacity (q_e) and removal efficiency (Removal %) are determined by Equations (1) and (2):^[37]

$$q_e = \frac{(C_0 - C_e) \cdot V}{m} \quad (1)$$

$$\text{Removal \%} = \frac{100 \cdot (C_0 - C_e)}{C_0} \quad (2)$$

where q_e (mg g⁻¹) is the adsorption capacity of the dye at equilibrium; C_0 (mg L⁻¹) is the initial dye concentration; C_e (mg L⁻¹) is the residual dye concentration at equilibrium; V (L) is the volume of dye solution used and m (g) is the mass of adsorbent.

Pseudo-first-order, pseudo-second-order, and intra-particle diffusion kinetic models were used to explore possible adsorption mechanisms and to determine the concentration of residual dye in solution at each time point.^[30]

The pseudo-first-order kinetic model equation is as follows:

$$\ln(q_e - q_t) = \ln q_e - k_1 t \quad (3)$$

The pseudo-second-order kinetic model equation is as follows:

$$\frac{1}{q_t} - \frac{1}{q_e} = \frac{1}{k_2 q_e^2 t} \quad (4)$$

The intra-particle diffusion kinetic model equation is as follows:

$$q_t = k_i t^{1/2} + C_i \quad (5)$$

where q_e (mg g⁻¹) is the adsorption capacity of dye at equilibrium, q_t (mg g⁻¹) is the adsorption capacity of dye at time t (min), C_i is the in-

tercept described the effects of boundary layer thickness, k_1 (min^{-1}), k_2 ($\text{g mg}^{-1} \text{min}^{-1}$) and k_3 ($\text{mg g}^{-1} \text{min}^{-1/2}$) are the adsorption rate constant of the three models, respectively.

In order to obtain the maximum adsorption capacity and adsorption isotherm of PI/COF-SO₃H-2.0 on MB, add 10 mg of PI/COF-SO₃H-2.0 to 100 mL of MB with an initial concentration of 20, 50, 100, 150, 200, 300, and 400 mg L^{-1} respectively. After reaching adsorption equilibrium, measure the concentration of residual dye in the solution and calculate the adsorption amount. The adsorption isotherms were analyzed using the Langmuir and Freundlich isotherm model.^[33]

The Langmuir isotherm model was expressed according to the following equation:

$$\frac{C_e}{q_e} = \frac{1}{K_L q_m} + \frac{C_e}{q_m} \quad (6)$$

The Freundlich isotherm model was expressed according to the following equation:

$$\log q_e = \log K_F + \frac{1}{n} \log C_e \quad (7)$$

where C_e (mg L^{-1}) is the concentration of dye in solution at equilibrium, q_e (mg g^{-1}) is the adsorption capacity of dye at equilibrium, K_L ($\text{dm}^3 \text{mg}^{-1}$) is the Langmuir constant, q_m (mg g^{-1}) is the Langmuir maximum adsorption capacity, K_F ($(\text{mg g}^{-1})^{1/n}$) is the Freundlich constant, and n indicates the Freundlich exponent.

In the rapid adsorption contrast experiment of PI/COF-SO₃H-2.0 and COF-SO₃H powder, 10 mg PI/COF-SO₃H-2.0, and 5.84 mg COF-SO₃H powder were immersed in 5 mL MB (20 mg L^{-1}) solution respectively and placed on a stirrer with a rotation speed of 200 rpm, until the adsorption equilibrium was reached. The concentration of residual dye in the solution at each time point was determined by UV-vis spectroscopy and the removal rate of MB was calculated.

The pH value of the solution affects the adsorption of MB by PI/COF-SO₃H-2.0. The pH value of the MB solutions adjusted to pH ranging from 3 to 11 by 0.1 M HCl or 0.1 M NaOH. Then 10 mg of PI/COF-SO₃H-2.0 was added to 200 mL of MB solutions (20 mg L^{-1}) with different pH values. After the adsorption equilibrium was reached, the concentration of residual dye in the solution was measured by UV-vis spectroscopy, and the adsorption amount of PI/COF-SO₃H-2.0 to MB was calculated.

Put the cylindrical PI/COF-SO₃H sponge with a diameter of 1.5 cm and a height of 1 cm into the syringe to make a simple filter device. The pH value of the filtered solution was 7 and the concentration of MB was 10 mg L^{-1} . After filtration, the concentration of residual dye in the filtrate was determined by UV-vis spectroscopy, and the removal efficiency of the dye was calculated according to Equation (2), and the flux was calculated by Equation (8):^[38]

$$\text{Flux} = \frac{V}{A \cdot t} \quad (8)$$

Where Flux ($\text{L h}^{-1} \text{m}^{-2}$) is the volume of the dye solution passing through the PI/COF-SO₃H sponge per unit time and unit area under self-gravity; A (m^2) is the cross-sectional area of the PI/COF-SO₃H sponge; t (h) is the time for the dye solution to filter; V (L) is the volume of dye solution that passes through the sample in time t .

Four simple filtration devices with PI/COF-SO₃H-2.0 as filters were connected in series as a whole to filter MB (10 mg L^{-1} , pH value was 7) solution continuously for 24 h. The concentration of residual dye in filtrate at each time point and the corresponding MB removal rate were determined by UV-vis spectroscopy.

In the recyclability experiment, all PI/COF-SO₃H sponges were washed with methanol containing 1 mM HCl several times after dye adsorption until completely desorbed as checked by the absence of any MB in the washing solution. The regenerated sponges could be reused after drying in a vacuum.

At room temperature, soak 10 mg of PI/COF-SO₃H-2.0 in 100 mL of FL solution (20 mg L^{-1} , pH value was 7), place it on a stirrer with a rotation speed of 200 rpm, until the adsorption equilibrium is reached, and the absorbance of the solution was measured by UV-vis spectroscopy. PI/COF-SO₃H-2.0 was used as a filter to filter the mixed solution of 10 mg L^{-1} MB and FL, and the absorbance of residual dye in the filtrate and the corresponding dye removal rate were measured by UV-vis spectroscopy.

Supporting Information

Supporting Information is available from the Wiley Online Library or from the author.

Acknowledgements

The authors acknowledge Deutsche Forschungsgemeinschaft (DFG) (SFB 1585, project A01) for supporting the work. Y.D. thanks the China Scholarship Council (CSC) for financing the research stay in Germany. Prof. Jürgen Senker is thanked for making available resources for measuring the ¹³C solid-state NMR.

Open access funding enabled and organized by Projekt DEAL.

Conflict of Interest

The authors declare no conflict of interest.

Author Contributions

Concepts and resources were generated by S.A.. C.D. designed experiments in consultation with S.A.. C.D. performed all experiments, and analyzed data. Y.D. performed filtration experiments with C.D.. The manuscript was written with the help of all coauthors.

Data Availability Statement

The data that support the findings of this study are available in the supplementary material of this article.

Keywords

adsorbent, covalent organic frameworks, filter, sponges, sustainable

Received: August 21, 2023
Revised: September 26, 2023
Published online: October 8, 2023

- [1] C. J. Doonan, D. J. Tranchemontagne, T. G. Glover, J. R. Hunt, O. M. Yaghi, *Nat. Chem.* **2010**, *2*, 235.
- [2] S. Wang, Y. Yang, Xu Liang, Y. Ren, H. Ma, Z. Zhu, J. Wang, S. Zeng, S. Song, X. Wang, Y. Han, G. He, Z. Jiang, *Adv. Funct. Mater.* **2023**, *33*, 2300386.
- [3] J. Li, S.-Y. Gao, J. Liu, S. Ye, Y. Feng, D.-H. Si, R. Cao, *Adv. Funct. Mater.* **2023**, 2305735.
- [4] Q. Sun, B. Aguila, Y. Song, S. Ma, *Acc. Chem. Res.* **2020**, *53*, 812.
- [5] H. Yang, L. Yang, H. Wang, Z. Xu, Y. Zhao, Y. Luo, N. Nasir, Y. Song, H. Wu, F. Pan, Z. Jiang, *Nat. Commun.* **2019**, *10*, 2101.

- [6] J. Li, X. Jing, Q. Li, S. Li, X. Gao, X. Feng, B. Wang, *Chem. Soc. Rev.* **2020**, *49*, 3565.
- [7] N. Keller, T. Bein, *Chem. Soc. Rev.* **2021**, *50*, 1813.
- [8] H. S. Sasmal, H. B. Aiyappa, S. N. Bhange, S. Karak, A. Halder, S. Kurungot, R. Banerjee, *Angew. Chem., Int. Ed.* **2018**, *130*, 11060.
- [9] K. Dey, S. Kunjattu H, A. M. Chahande, R. Banerjee, *Angew. Chem., Int. Ed.* **2020**, *132*, 1177.
- [10] L. Huang, J. Yang, Y. Zhao, H. Miyata, M. Han, Q. Shuai, Y. Yamauchi, *Chem. Mater.* **2023**, *35*, 2661.
- [11] a) M. Di, X. Sun, L. Hu, L. Gao, J. Liu, X. Yan, X. Wu, X. Jiang, G. He, *Adv. Funct. Mater.* **2022**, *32*, 2111594; b) S. Hao, T. Zhang, S. Fan, Z. Jia, Y. Yang, *Chem. Eng. J.* **2021**, *421*, 129750.
- [12] Y. Li, Q. Wu, X. Guo, M. Zhang, B. Chen, G. Wei, X. Li, X. Li, S. Li, L. Ma, *Nat. Commun.* **2020**, *11*, 599.
- [13] C. Fan, H. Wu, J. Guan, X. You, C. Yang, X. Wang, L. Cao, B. Shi, Q. Peng, Y. Kong, Y. Wu, N. A. Khan, Z. Jiang, *Angew. Chem., Int. Ed.* **2021**, *60*, 18051.
- [14] C. Ding, M. Breunig, J. Timm, R. Marschall, J. Senker, S. Agarwal, *Adv. Funct. Mater.* **2021**, *31*, 2106507.
- [15] A. K. Mohammed, S. Usgaonkar, F. Kanheerampockil, S. Karak, A. Halder, M. Tharkar, M. Addicoat, T. G. Ajithkumar, R. Banerjee, *J. Am. Chem. Soc.* **2020**, *142*, 8252.
- [16] a) F. Li, L.-G. Ding, B.-J. Yao, N. Huang, J.-T. Li, Q.-J. Fu, Y.-B. Dong, *J. Mater. Chem. A* **2018**, *6*, 11140; b) Z. Liu, H. Wang, J. Ou, L. Chen, M. Ye, *J. Hazard. Mater.* **2018**, *355*, 145.
- [17] a) Q. Sun, B. Aguila, J. A. Perman, T. Butts, F.-S. Xiao, S. Ma, *Chem* **2018**, *4*, 1726; b) J. Li, Y. Yang, W. Ma, G. Li, Q. Lu, Z. Lin, *J. Hazard. Mater.* **2021**, *411*, 125190.
- [18] Y. Xu, T. Wu, Z. Cui, L. Kang, Y. Cai, J. Li, D. Tian, *Sep. Purif. Technol.* **2022**, *303*, 122275.
- [19] S. Karak, K. Dey, A. Torris, A. Halder, S. Bera, F. Kanheerampockil, R. Banerjee, *J. Am. Chem. Soc.* **2019**, *141*, 7572.
- [20] a) M. Dilamian, M. Joghataei, Z. Ashrafi, C. Bohr, S. Mathur, H. Maleki, *Appl. Mater. Today* **2021**, *22*, 100964; b) X. Xie, Z. Zheng, X. Wang, D. Lee Kaplan, *ACS Nano* **2021**, *15*, 1048; c) X. Dong, L. Cao, Y. Si, B. Ding, H. Deng, *Adv. Mater.* **2020**, *32*, 1908269; d) Q. Fu, Y. Si, C. Duan, Z. Yan, L. Liu, J. Yu, B. Ding, *Adv. Funct. Mater.* **2019**, *29*, 1808234.
- [21] a) S. Jiang, B. Uch, S. Agarwal, A. Greiner, *ACS Appl. Mater. Interfaces* **2017**, *9*, 32308; b) G. Duan, S. Jiang, V. Jérôme, J. H. Wendorff, A. Fathi, J. Uhm, V. Altstädt, M. Herling, J. Breu, R. Freitag, S. Agarwal, A. Greiner, *Adv. Funct. Mater.* **2015**, *25*, 2850.
- [22] K. Dey, S. Mohata, R. Banerjee, *ACS Nano* **2021**, *15*, 12723.
- [23] X. H. Xiong, Z. W. Yu, L. L. Gong, Y. Tao, Z. Gao, L. Wang, W. H. Yin, L. X. Yang, F. Luo, *Adv. Sci.* **2019**, *6*, 1900547.
- [24] a) X. Liao, M. Dulle, J. M. De Souza E Silva, R. B. Wehrspohn, S. Agarwal, S. Förster, H. Hou, P. Smith, A. Greiner, *Science* **2019**, *366*, 1376; b) K. Ruan, Y. Guo, J. Gu, *Macromolecules* **2021**, *54*, 4934.
- [25] Y. Han, Q. Zhang, N. Hu, X. Zhang, Y. Mai, J. Liu, X. Hua, H. Wei, *Chin. Chem. Lett.* **2017**, *28*, 2269.
- [26] S. Kandambeth, A. Mallick, B. Lukose, M. V. Mane, T. Heine, R. Banerjee, *J. Am. Chem. Soc.* **2012**, *134*, 19524.
- [27] P. Pachfule, S. Kandambeth, A. Mallick, R. Banerjee, *ChemComm* **2015**, *51*, 11717.
- [28] L. Liu, L. Yin, D. Cheng, S. Zhao, H.-Y. Zang, N. Zhang, G. Zhu, *Angew. Chem., Int. Ed.* **2021**, *133*, 15001.
- [29] a) C. Li, P. Guggenberger, S. W. Han, W. L. Ding, F. Kleitz, *Angew. Chem., Int. Ed.* **2022**, *61*, e202206564; b) Y. Chen, M. Hanshe, Z. Sun, Y. Zhou, C. Mei, G. Duan, J. Zheng, E. Shiju, S. Jiang, *Int. J. Biol. Macromol.* **2022**, *207*, 130.
- [30] a) C.-H. Wu, *J. Hazard. Mater.* **2007**, *144*, 93; b) D.-S. Kim, S.-B. Lim, *Sep. Purif. Technol.* **2020**, *250*, 117259.
- [31] a) J. Huo, B. Luo, Y. Chen, *ACS Omega* **2019**, *4*, 22504; b) X. Ma, S. Zhao, Z. Tian, G. Duan, H. Pan, Y. Yue, S. Li, S. Jian, W. Yang, K. Liu, S. He, S. Jiang, *Chem. Eng. J.* **2022**, *446*, 136851.
- [32] a) S. Jiang, T. Yu, R. Xia, X. Wang, M. Gao, *Mater. Chem. Phys.* **2019**, *232*, 374; b) X. Zhong, Z. Lu, W. Liang, B. Hu, *J. Hazard. Mater.* **2020**, *393*, 122353.
- [33] a) L. You, K. Xu, G. Ding, X. Shi, J. Li, S. Wang, J. Wang, *J. Mol. Liq.* **2020**, *320*, 114456; b) B.-C. Hu, H.-R. Zhang, S.-C. Li, W.-S. Chen, Z.-Y. Wu, H.-W. Liang, H.-P. Yu, S.-H. Yu, *Adv. Funct. Mater.* **2023**, *33*, 2207532.
- [34] a) R. Ezzati, *Chem. Eng. J.* **2020**, *392*, 123705; b) S. S. A. Alkurdi, R. A. Al-Juboori, J. Bundschuh, L. Bowtell, A. Marchuk, *J. Hazard. Mater.* **2021**, *405*, 124112.
- [35] a) D. Chen, J. Chen, X. Luan, H. Ji, Z. Xia, *Chem. Eng. J.* **2011**, *171*, 1150; b) K. Azam, N. Shezad, I. Shafiq, P. Akhter, F. Akhtar, F. Jamil, S. Shafique, Y.-K. Park, M. Hussain, *Chemosphere* **2022**, *306*, 135566.
- [36] a) S. Kandambeth, B. P. Biswal, H. D. Chaudhari, K. C. Rout, S. Kunjattu H, S. Mitra, S. Karak, A. Das, R. Mukherjee, U. K. Kharul, R. Banerjee, *Adv. Mater.* **2017**, *29*, 1603945; b) C. Mao, S. Zhao, P. He, Z. Wang, J. Wang, *Chem. Eng. J.* **2021**, *414*, 128929.
- [37] a) G.-H. Ning, Z. Chen, Q. Gao, W. Tang, Z. Chen, C. Liu, B. Tian, X. Li, K. P. Loh, *J. Am. Chem. Soc.* **2017**, *139*, 8897; b) Y. Chen, S. Li, X. Li, C. Mei, J. Zheng, E. Shiju, G. Duan, K. Liu, S. Jiang, *ACS Nano* **2021**, *15*, 20666.
- [38] Y. Liu, W. Li, C. Yuan, L. Jia, Y. Liu, A. Huang, Y. Cui, *Angew. Chem., Int. Ed.* **2022**, *61*, e202113348.